ANALYSIS OF THE DYNAMIC COEFFICIENTS OF THRUST BEARINGS WITH HYDRODYNAMIC LUBRICATION

Leonardo Carpinetti Vieira, leonardocv@fem.unicamp.br
Katia Lucchesi Cavalca, katia@fem.unicamp.br
Laboratory of Rotating Machinery – Faculty of Mechanical Engineering – Postal Box 6122
University of Campinas – UNICAMP - 13083-970, Campinas, SP, Brazil

Abstract. *In order to design an effective thrust bearing, it is very important to know how the pressure is generated within the oil film and the magnitude of the load capacity transmitted from the collar to the bearing throughout the fluid. This lubricant fluid, which can be modeled as a spring-damper system with negligible mass, has a fundamental importance to avoid contact between solid parts with axial relative motion, preventing friction, wear and failure of elements on a rotating machine. To analyze this problem, the Reynolds' Equation must be solved so that the distribution of pressure on the sections under hydrodynamic lubrication is obtained and the total load capacity of the bearing can be calculated. The solution of this fundamental equation is reached by using a Finite Volume Method in polar coordinates, solving a balance of fluid flows in each control volume of the mesh, which allows the analysis of film thickness discontinuities that exist due to the bearing grooves. Knowing the distribution of pressure and the total load capacity of the lubricant, it is possible to calculate the equivalent stiffness and damping coefficients of the fluid film. Constant fluid viscosity and density are assumed as well as the fact that the collar attached to the shaft is always parallel to the thrust bearing. For this reason, only direct coefficients in the axial direction are calculated. This kind of analysis is very important to allow the prediction of the dynamic behavior of the shaft-lubricant-bearing system, improving the parameters of investigation of rotating machines with thrust bearings.*

Keywords*: Thrust Bearings; Finite Volume Method; Reynolds' Equation; Hydrodynamic Lubrication; Dynamic Coefficients.*

1. INTRODUCTION

The study of rotating machinery plays a very important role in the field of structures and machines, as this type of equipment has its own typical phenomena while in operation. The existence of a rotating element supported by bearings and transmitting power creates a range of problems which can occur in several different equipments, such as compressors, turbines, pumps, engines, turbochargers and so on. Such machines are usually part of great facilities or energy generators and any unexpected maintenance may result in large financial losses. For this reason, a wider knowledge of the phenomena that may happen in rotating machinery, more specifically between the fixed and rotating components, is required.

In the specific case of a shaft under axial external forces, effective thrust bearings are required to avoid contact between solid parts and, consequently, wear and failure. Hydrodynamic bearings may prevent such contacts due to the lubricant fluid film in the interface of the moving parts, which must be able to provide load capacity with the least energy waste as possible and without introducing undesired instabilities. Large axial movements of the shaft can be avoided due to the pressures generated within the oil present between the bearing and the moving collar, which rotates with the shaft. In order to ensure the correct functioning of the system, the clearance containing the lubricant must be extremely small, in the order of micrometers, and the bearing must have several pads separated by grooves that provide the oil, searching to avoid cavitation and to improve the heat dissipation.

The study of lubrication in rotating machinery started during the 19th century, when scientists such as Petrov (1883), Tower (1885) and Reynolds (1886) gave a great contribution to the tribology. Reynolds was responsible for writing the differential equation that defines the pressure profile between two surfaces with relative motion. This equation was obtained applying some simplifications to the Navier-Stokes Equations and it is still the basis of modern lubrication theory.

During the 20th century, several scientists attempted to solve the Reynolds Equation by means of numerical methods. Pinkus and Lynn (1958) solved this equation for sector thrust bearings using the Finite Difference Method (FDM). Nevertheless, due to computational limitations, they could only use a 7 x 7 mesh, which may have introduced errors in the values of the integrated pressure. Two years earlier, Pinkus had already solved the Reynolds' Equation for elliptical journal bearings, also by using the FDM. In 1981, Singhal discussed in his paper some relaxation methods, the Jacobi-Method and the Gauss-Seidel Method, analyzing the numerical convergence and trying to reduce the computational time. Koç (1990) used the FDM with Lagrange Polynomials to solve the Reynolds Equation. Vieira and Cavalca (2009) and Vieira et al. (2010) used the FDM to calculate the generated pressure on thrust bearings, analyzed the influence of several operating parameters on the load capacity of the bearing and searched for an optimized bearing pad ramp size. Other authors, on the other hand, used the Finite Volume Method, also called FVM, (which, unlike the FDM, allows the introduction of fluid film discontinuities) to solve this equation, such as Kogure et al. (1983) and Jang et al. (2006), who used a coordinate transformation in order to align the fluid film discontinuities to the mesh.

Other authors focused their efforts on the calculation of the equivalent dynamic coefficients of the lubricant. Lund (1987) reviewed in his paper the concept of stiffness and damping coefficients for journal bearings. Storteig and White (1999) calculated the crossed stiffness and damping coefficients for thrust bearings and analyzed the effects of the thrust bearings on lateral vibration. They used the Finite Elements Method to obtain the pressure distribution on the bearing. Zhu and Zhang (2003) used a non-linear model to study the transient response of thrust bearings with hydrodynamic lubrication. Jang et al. (2006) also used the Finite Elements Model, but to study the dynamic behavior of a system with journal and thrust bearings in a computer hard disk. In 2006, Jang and Lee, calculated the dynamic coefficients by using the perturbations method, the same approach applied in the present paper.

The present paper attempts to perform a preliminary analysis of thrust bearings under hydrodynamic lubrication. Both the axial load capacity and the dynamic behavior of thrust bearings are analyzed. A FVM, which allows the analysis of fluid film discontinuities, such as thrust bearing grooves, is used to solve the Reynolds Equation and to obtain the load capacity of this type of bearings. A balance of the fluid flows inside each control volume is applied with help from the Bernoulli Equation, according to the model suggested by Arghir et al. (2002), allowing the analysis of rapid pressure variations due to the discontinuities. Having the load capacity, it is possible to calculate both the direct stiffness and damping equivalent coefficients of the lubricant fluid present between the bearing and the rotating collar.

At first, a result of pressure distribution obtained with the model with film discontinuities (bearing grooves) by FVM is compared to the result obtained with a FDM code, earlier implemented by the authors (Vieira and Cavalca (2009) and Vieira et al., 2010), without film discontinuities. To verify the algorithm performance, both methods, FVM and FDM, are applied in similar conditions, in which the influence of the grooves is not very expressive and the potential of the FVM is not completely used. This comparison validates the calculation method used. Although the method suggested by Arghir et al. (2002) allows further analysis of film discontinuities, such as the analysis of pocket thrust bearings or "Rayleigh-Step" bearing pads, the objective of the present paper is to perform a preliminary analysis of the results obtained without the consideration of the influence of concentrated inertia effect or the temperature influence. Nonetheless, the authors recognize the importance of such influences and intend to analyze these influences in future works.

Secondly, the dynamic coefficients of bearings with different geometrical parameters and different fluid viscosities are calculated and compared.

Finally, the coefficients obtained are compared to the coefficients obtained by Zhu and Zhang (2003), attempting to validate the results of dynamic coefficients obtained with the implemented code.

2. THEORY AND RESULTS

2.1 Coordinate Systems and Bearing Pads

The Reynolds' Equation solved in this paper is used in Polar Coordinates. Figure 1 shows the geometry of the pad of a thrust bearing in both Polar and Cartesian co-ordinate systems. The coordinate r is in the radial direction with the reference in the center of the bearing; the coordinate θ is the circumferential direction and increases clock-wisely. It is known that the Cartesian coordinates are related to the polar ones as follows: $y = r\theta$ and $z = r$.

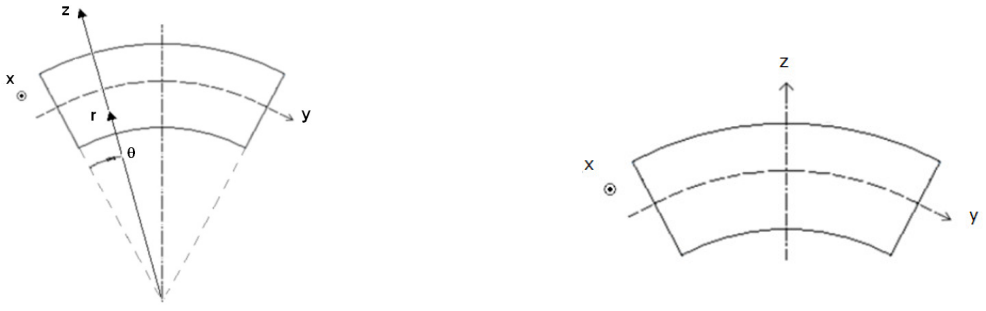

(a) (b)

Figure 1. (a) Polar and (b) Cartesian coordinates in a pad of a sector thrust bearing

The shape of the bearing pad, as assumed in the case with no bearing grooves considered, as well as the fluid film shape, can be seen in Fig. 2 (a) and (b). The inner radius of the pad is given by r_{inner}, the outer radius is given by r_{outer}, resulting, as a consequence, in $b = r_{outer} - r_{inner}$. The angular span of each pad is given by θ_o and the angular size of the ramp is given by θ_{ramp}. All bearing pads considered in this paper have a ratio of $\theta_{ramp} / \theta_o = 3/4$, what, according to shown in Vieira et al. (2010), is the ratio that provides an optimized load capacity. It is important to notice that the flat surface in Fig. 2 (b) rotates in the same direction of θ. This surface is the collar. The bearing (upper surface) has no load capacity whether the shaft rotates in the opposite direction. The oil shape, considering the grooves can be seen in

Fig. 2 (c). In Fig. 2 (b) and Fig. 2 (c), h_o is the minimum film thickness and $h_{\max}$ is the maximum film thickness. The difference between these two values of film thickness is given by $s_h = h_{\max} - h_o$.

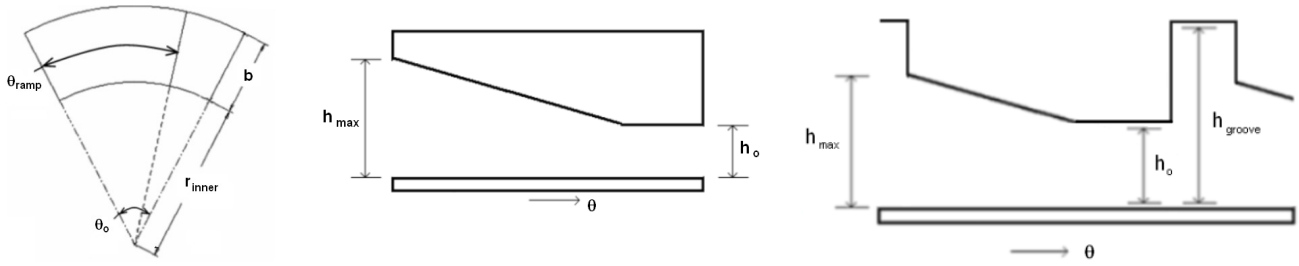

(a) (b) (c)

Figure 2. (a) Bearing pad; (b) Fluid film thickness for the case with no grooves; (c) Fluid film thickness for the case with grooves

2.2 Reynolds' Equation and Assumptions

The differential equation which governs the pressure distribution in the lubricant fluid present in the clearance between a thrust bearing and the collar attached to the shaft, the Reynolds' Equation, is given in Eq. (1). As mentioned before, it is usually written in polar coordinates when studying thrust bearings.

In Eq. (1), p is the pressure generated within the fluid, r and θ are the polar co-ordinates, as shown in Fig. 1, h is the film thickness, η is the absolute viscosity of the lubricant and v_θ is the velocity of the collar attached to the shaft, in the θ direction. Constant temperature, viscosity and density of the fluid are assumed. The velocity of the fluid in contact with the collar surface in the radial direction is null, since any movement of the collar in this direction is neglected. Hydrodynamic lubrication is considered and the effect of temperature on the lubricant fluid viscosity is not considered. As commonly used in problems related to bearings, the pressure is assumed as being atmospheric along the outer boundary of the bearing. When the grooves are not considered and the bearing pad is analyzed separately, the pressure is atmospheric also in the positions with $\theta = 0$ and $\theta = \theta_o$. Unlike the assumptions made in analytical solutions solved by several authors (such as Hamrock et al., 2005, for example), side leakages of fluid are not neglected in numerical solutions.

The Reynolds' Equation may also be written based on the fluid flows. Equation (2), written as function of the fluid flows in both radial and angular directions, is equivalent to Eq. (1) and it is the basis for the numerical solution obtained in this paper. It should be pointed out that in the calculation of the damping coefficients, the term $\partial h / \partial t$, which considers the variation of the fluid film in time, must be considered in Eq. (1) and in Eq. (2).

$$\frac{1}{r}\frac{\partial}{\partial\theta}\left(h^3\frac{\partial p}{\partial\theta}\right)+\frac{\partial}{\partial r}\left(h^3 r\frac{\partial p}{\partial r}\right)=6v_\theta\eta\frac{\partial h}{\partial\theta} \tag{1}$$

$$\frac{1}{r}\frac{\partial q'_{pad}}{\partial\theta}+\frac{\partial q'_{lat}}{\partial r}=0 \tag{2}$$

The fluid flow per unit width in the radial direction, q'_{lat}, can be seen in Eq. (3), while the flow per unit length in the angular direction, q'_{pad}, is seen in Eq. (4). In this last equation, the subscript *c* is related to the moving collar. Since the bearing is stationary, the velocities related to it are neglected in both equations.

$$q'_{lat}=-\frac{h^3}{12\eta}\frac{\partial p}{\partial r} \tag{3}$$

$$q'_{pad}=-\frac{h^3}{12\eta}\frac{1}{r}\frac{\partial p}{\partial\theta}+\frac{v_{\theta c}}{2}h \tag{4}$$

2.3 Finite Volume Method and Calculation of the Pressure Distribution

The numerical method used to solve the Reynolds' Equation is the Finite Volume Method, based on the solution of Arghir et al. (2002). This solution is based on a balance of fluid flows in every control volume of the mesh. Figure 3 shows a control volume in the mesh built in polar coordinates. In this figure, the index i is related to the position of a

node of the mesh in the radial direction, while the index j is related to the position of a node in the angular direction.

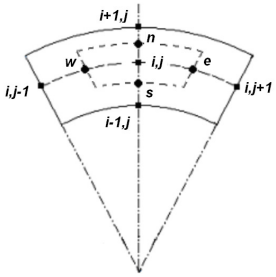

Figure 3. Control volume in polar coordinates

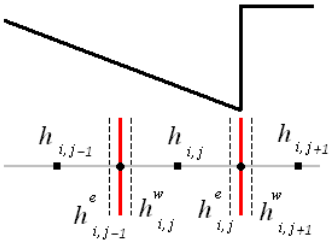

Figure 4. Control volume and fluid film discontinuities

In this solution, the film discontinuities must always be coincident with the boundary of a control volume (the film thickness in the east or west position of the cell), as seen in Fig. 4:

Equation (2) can be rewritten as a function of the fluid flows across the boundaries of the control volumes in north, south, east and west:

$$q'^{w}_{i,j}\partial r + q'^{s}_{i,j} r\,\partial\theta - q'^{e}_{i,j}\partial r - q'^{n}_{i,j} r\,\partial\theta = 0 \tag{5}$$

The relationship between the flows of adjacent cells may be written as seen in the set of expressions written in Eq. (6), knowing that the flows at the east and west sides of each cell are related to q'_{pad} (angular), and the flows at north and south are related to q'_{lat} (radial).

$$\begin{aligned} q'^{e}_{i,j} &= q'^{w}_{i,j+1} \qquad q'^{w}_{i,j} = q'^{e}_{i,j-1} \\ q'^{n}_{i,j} &= q'^{s}_{i+1,j} \qquad q'^{s}_{i,j} = q'^{n}_{i-1,j} \end{aligned} \tag{6}$$

The terms of Eq. (6) may be rewritten in function of q'_{pad} and q'_{lat}. Substituting Eq. (4) into the term $q'^{e}_{i,j} = q'^{w}_{i,j+1}$, for example, the following expression is obtained:

$$\left[-\left(\frac{h^3}{12\eta r}\right)^{e}_{i,j} \frac{p^{e}_{i,j} - p_{i,j}}{(\theta_{i,j+1} - \theta_{i,j})/2} + \frac{v_{\theta c} h^{e}_{i,j}}{2}\right] = \left[-\left(\frac{h^3}{12\eta r}\right)^{w}_{i,j+1} \frac{p_{i,j+1} - p^{w}_{i,j+1}}{(\theta_{i,j+1} - \theta_{i,j+1})/2} + \frac{v_{\theta c} h^{w}_{i,j+1}}{2}\right] \tag{7}$$

Introducing the term $b^{w}_{i,j+1}$, described in Eq. (8), and rearranging Eq. (7), the expression written in Eq. (9) is obtained:

$$b^{w}_{i,j+1} = \left[\left(\frac{h^3}{12\eta r}\right)^{w}_{i,j+1} \frac{1}{\Delta\theta/2}\right] \tag{8}$$

$$b^{e}_{i,j} p^{e}_{i,j} + b^{w}_{i,j+1} p^{w}_{i,j+1} = b^{e}_{i,j} p_{i,j} + b^{w}_{i,j+1} p_{i,j+1} + \left[\frac{v_{\theta c}(h^{e}_{i,j} - h^{w}_{i,j+1})}{2}\right] \tag{9}$$

To analyze the abrupt pressure change that occurs when fluid film discontinuities are considered, Arghir et al. (2002) introduced the use of a simplified and rearranged Bernoulli Equation as seen in Eq. (10):

$$p^{w}_{i,j+1} = p^{e}_{i,j} - A_{i,j+1/2} \tag{10}$$

in which $V^{e}_{i,j} = \dfrac{q'^{e}_{i,j}}{h^{e}_{i,j}}$ and $V^{w}_{i,j+1} = \dfrac{q'^{w}_{i,j+1}}{h^{w}_{i,j+1}}$ are fluid velocities and $A_{i,j+1/2} = \dfrac{\rho(V^{w}_{i,j+1})^2}{2} - \dfrac{\rho(V^{e}_{i,j})^2}{2}$. It is important to mention once again that, since the present approach is a preliminary work implementing the model proposed by Arghir et al. (2002), with the objective to compare the results obtained with this method with another model and analyze some results of dynamic coefficients obtained for different bearing pad geometries, the term of concentrated inertia is neglected, as performed by Arghir et al. (2002) on part of their results, focusing more on the use of the generalized

Bernoulli equation written immediately before and after a film discontinuity to analyze the pressure drop at this region due to the kinetic energy variation, not considering the influence of viscous effects.

Substituting Eq. (9) in Eq. (10), the following expression for the pressure at the east of the control volume is obtained:

$$p_{i,j}^{e} = \left[b_{i,j}^{e} p_{i,j} + b_{i,j+1}^{w} p_{i,j+1} + b_{i,j}^{w} A_{i,j+1/2} + \frac{v_{\theta c}(h_{i,j}^{e} - h_{i,j+1}^{w})}{2} \right] \Big/ \left[b_{i,j}^{e} + b_{i,j+1}^{w} \right] \tag{11}$$

Applying this same procedure to the other terms of Eq. (6), the values of pressure at the western, northern and southern boundaries of each cell can be calculated.

Returning to Eq. (5), substituting the expressions for the fluid flows, the following equation is obtained:

$$b_{i,j}^{w}\left(p_{i,j}^{w} - p_{i,j}\right)\partial r + \frac{v_{\theta c} h_{i,j}^{w}}{2}\partial r + b_{i,j}^{s}\left(p_{i,j}^{s} - p_{i,j}\right)r_{i,j}\partial\theta - b_{i,j}^{e}\left(p_{i,j} - p_{i,j}^{e}\right)\partial r + \frac{v_{\theta c} h_{i,j}^{e}}{2}\partial r - b_{i,j}^{n}\left(p_{i,j} - p_{i,j}^{n}\right)r_{i,j}\partial\theta = 0 \tag{12}$$

After the substitution of the values of the pressures $p_{i,j}^{e}$, $p_{i,j}^{w}$, $p_{i,j}^{n}$ and $p_{i,j}^{s}$, the expression for the calculation of the pressure at the center of one control volume is finally found in Eq. (13):

$$p_{i,j} = \frac{b_{i,j}^{e}\left(p_{i,j}^{e}\right)\partial r + b_{i,j}^{w}\left(p_{i,j}^{w}\right)\partial r + b_{i,j}^{n}\left(p_{i,j}^{n}\right)r_{i,j}\partial\theta + b_{i,j}^{s}\left(p_{i,j}^{s}\right)r_{i,j}\partial\theta - \left[\frac{v_{\theta c}(h_{i,j}^{e} - h_{i,j}^{w})\partial r}{2}\right]}{b_{i,j}^{e}\partial r + b_{i,j}^{w}\partial r + b_{i,j}^{n} r_{i,j}\partial\theta + b_{i,j}^{s} r_{i,j}\partial\theta} \tag{13}$$

Once the pressure on every control volume has been calculated, the axial load capacity of the bearing may be obtained by integrating this pressure along the entire area of the bearing pads and grooves (if the grooves are considered in the calculations). Equation (14) shows the expression used for this calculation.

$$W = \int\int pr\,\partial\theta\,\partial r \tag{14}$$

2.4 Calculation of Stiffness and Damping Coefficients

Having calculated the pressure distribution and load capacity of the bearing, it is possible to calculate the equivalent stiffness and damping coefficients of the lubricant fluid, that can be considered as analogous to a spring-damper system, as seen in Fig. 5. The mass of the fluid is neglected, since the amount of fluid present between the bearing and the collar is extremely small.

The direct stiffness coefficient, K_{xx}, can be calculated by introducing small perturbations to the equilibrium position, ∂x, as seen in Eq. (15):

$$K_{xx} = \frac{\partial W}{\partial x} \tag{15}$$

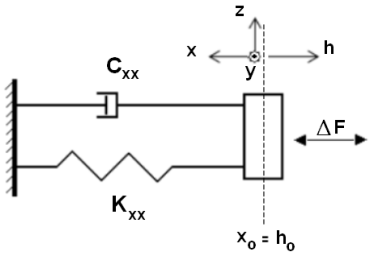

Figure 5. Spring-damper system representing the lubricant fluid

The damping coefficient is calculated by introducing the term of the fluid film thickness variation in time, $\partial h / \partial t$, in Eq. (2). Rearranging Eq. (2) after introducing $\partial h / \partial t$, Eq. (16) is obtained. The load capacity of the bearing is calculated again based on this equation and the direct damping coefficient can be calculated by Eq. (17).

$$\frac{1}{r}\frac{\partial q'_{pad}}{\partial\theta} + \frac{\partial q'_{lat}}{\partial r} = \frac{\partial h}{\partial t} \tag{16}$$

$$C_{xx} = \frac{\partial W}{\partial \dot{x}} \tag{17}$$

2.5 Results and General Comments

In the following sections, the results for pressure distribution and stiffness and damping coefficients are presented and analyzed. Bearings with and without grooves are compared at first. Then, coefficients for bearings with different geometries and different fluid viscosity values are analyzed.

2.5.1 Comparison between cases with and without grooves

The first results analyzed were the results obtained for bearings considering grooves (FVM analysis) and bearings without them (FDM analysis). In the second case, the pressure distribution is calculated for one single bearing pad and its load capacity is multiplied by the number of pads in order to obtain the total load capacity of the bearing.

Table 1 shows the geometrical data for the bearing used in the simulations and the viscosity of the lubricant fluid considered. The grid was built in a way that the dimensionless distance between two adjacent nodes is approximately $9x10^{-3}$ in both radial and angular directions. This value was used searching a compromise between computational time and accuracy of the results. Table 2 shows the results obtained for both cases and a comparison between them.

Table 1. Thrust Bearing and Fluid Data

Data	Value	Data	Value
r_{outer}	0,0135 m	θ_o	20°
r_{inner}	0,0045 m	N	50000 RPM
h_o	10 μm	s_h	10 μm
η	0.012 Ns/m^2		

Table 2: Results

	W_{total}	$\theta_{\max dim less}$	$R_{\max}$	$p_{\max}$
Grooves (FVM)	610,12 N	0,62	0,73	6,98 MPa
No grooves (FDM)	626,56 N	0,63	0,73	7,03 MPa
Difference	2,62 %	1,71 %	0 %	0,71 %

Equation 18 gives the expressions for the dimensionless positions of the maximum pressure both in the radial and angular directions.

$$R_{\max} = \frac{r_{\max} - r_{inner}}{b} \qquad \theta_{\max dim less} = \frac{\theta_{\max}}{\theta_o} \tag{18}$$

Comparing the results shown in Table 2, it can be seen that the load capacity and the pressure peak are slightly higher for the case in which grooves are not considered. The axial load capacity obtained in the simulation that does not consider grooves is around 2,6% higher than the one calculated with bearing grooves. The results of pressure distribution for the cases with bearing grooves and without grooves are in Fig. 6 and Fig. 7, respectively. In the case with grooves (Fig. 6), the pressure distribution is calculated for the entire bearing, while in the case with no grooves, the pressure at bearing pad is calculated and multiplied by the number of pads.

The results in Table 2, also demonstrate that the position of the peak pressure in the angular direction slightly changes when grooves are considered. The position of the peak pressure on the radial direction, on the other hand, remains practically the same. This may be explained by the fact that the boundary conditions at $r = r_{outer}$ and $r = r_{inner}$ considered in both cases are the same (pressure equals the atmospheric pressure), but the boundary conditions at $\theta = 0°$ and $\theta = \theta_o$ are different (when the grooves are considered, the pressure cannot be set as atmospheric and is calculated).

Figure 8 shows the pressure profile (at $R = R_{\max}$) obtained for one bearing pad in the case that considers the grooves. The red star in both figures shows the position of the end of the pad. Figure 9 shows the pressure profile for the case in which the grooves are not considered.

The results shown in Fig. 8 and Fig. 9, demonstrate that, unlike what happens at the second case, the pressure at the beginning and at the end of the pad at the first case is not null. Also, the pressure on the groove is mostly equal zero (calculated pressure values that are negative are set zero, since cavitation is not considered as the bearing is submerged in oil), as one can see from Fig. 10.

Comparing the results obtained with both methods, the FVM based on the proposal of Arghir et al. (2002), which allows the consideration of grooves, and the FDM, which does not allow the consideration of fluid film discontinuities, one can see that the results obtained were very similar. The pressure at the end and at the beginning of the bearing pads at the case with grooves is slightly different of zero due to numerical calculation, since the pressure at the groove is

equal zero, but the pressure above the pad is different of zero, resulting in values close to zero, but not null, at the nodes close to the grooves.

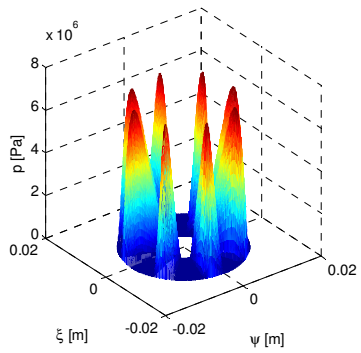

Figure 6. Pressure distribution for the case with grooves

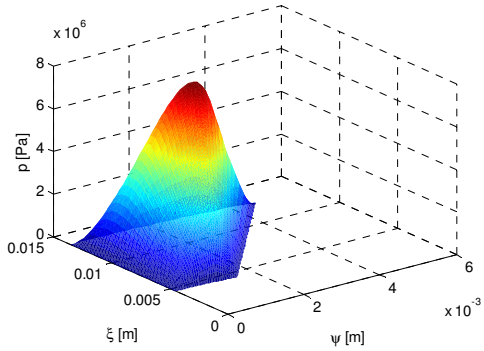

Figure 7. Pressure distribution for the case without grooves

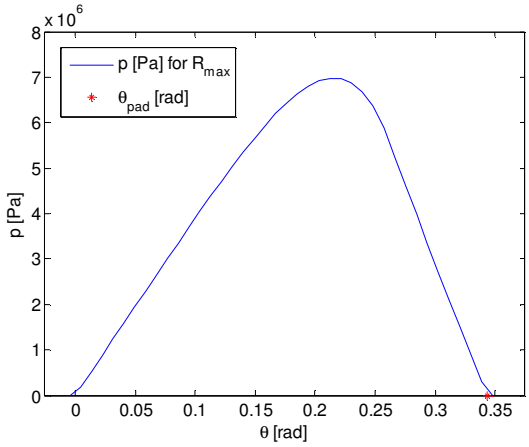

Figure 8. Pressure profile for one bearing pad in the case with the consideration of grooves

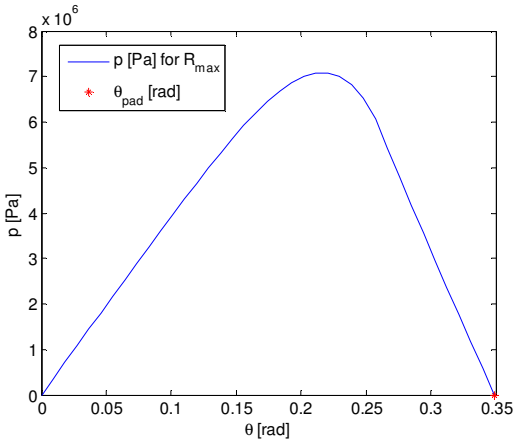

Figure 9. Pressure profile for one bearing pad in the case without the consideration of grooves

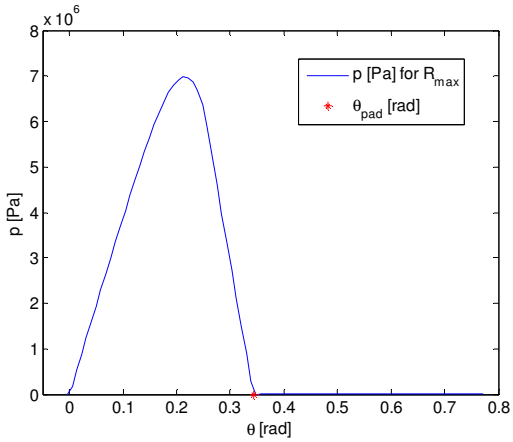

Figure 10. Pressure profile for one bearing pad and one groove

2.5.2 Stiffness and Damping Coefficients

Figure 11 and Fig. 12 show, respectively, the direct stiffness and damping coefficients as function of the speed of rotation of the collar, considering only the case of bearings with grooves. The calculations considered a fixed applied axial load of 100N. The required film thickness necessary to support such axial load at each speed was calculated before obtaining the dynamic coefficients.

An analysis of the dynamic coefficients of bearings with different angular pad sizes was performed. Figure 11 and Fig. 12 show the results of stiffness and damping coefficients obtained for bearings with four different values of θ_o. Figure 11 shows that smaller bearing pads result in higher stiffness coefficients. The reason for this behavior is that pads with smaller values of θ_o work with smaller values of film thickness than the bearings with longer pads in order to support the same axial load of 100N. The behavior observed in Fig. 12, however, shows that longer bearing pads result in greater values of damping coefficients.

Such behavior may be explained by the fact that thinner thicknesses result in stiffer bearings; a stiffer system implies that the displacements are lower, implying lower velocities, hence lower damping forces. The behavior of both stiffness and damping coefficients seen in Fig. 11 to Fig. 12 is similar to the behavior of the direct coefficients (in the vertical direction) calculated for cylindrical journal bearings, as seen in Machado and Cavalca (2009), following the typical behavior of coefficients of hydrodynamic bearings in general.

Figure 13 shows the minimum film thickness as function of the speed of the shaft for all four different values of θ_o. The behavior obtained for all the cases is similar, with the film thickness increasing as the speed of the shaft increases. Once again, one can notice that the bearing with smaller pads requires thinner film thicknesses to support the applied load of 100N.

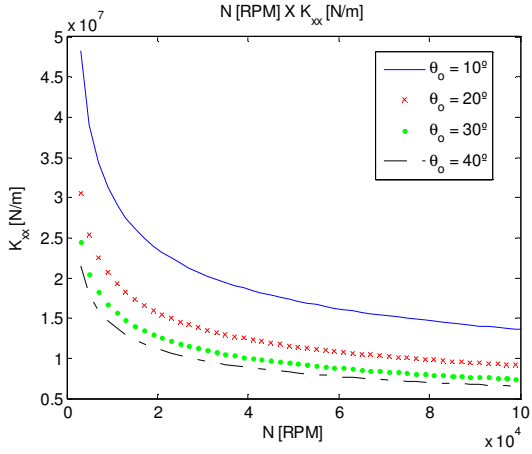

Figure 11. Stiffness coefficients as function of the speed of the shaft obtained for different values of θ_o

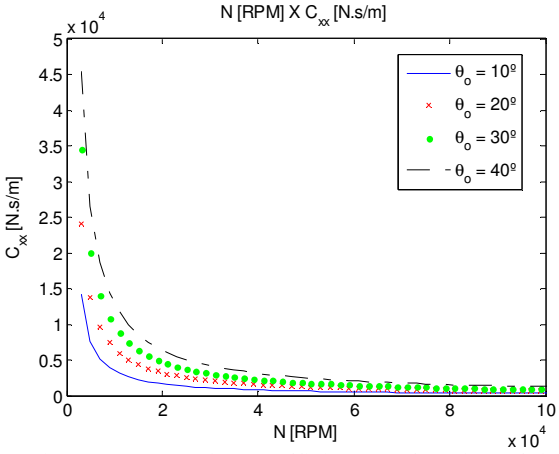

Figure 12. Damping coefficients as function of the speed of the shaft obtained for different values of θ_o

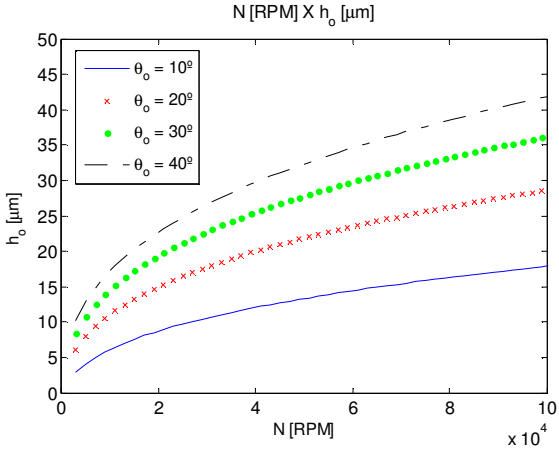

Figure 13. Minimum film thickness as function of the speed of the shaft obtained for different values of θ_o

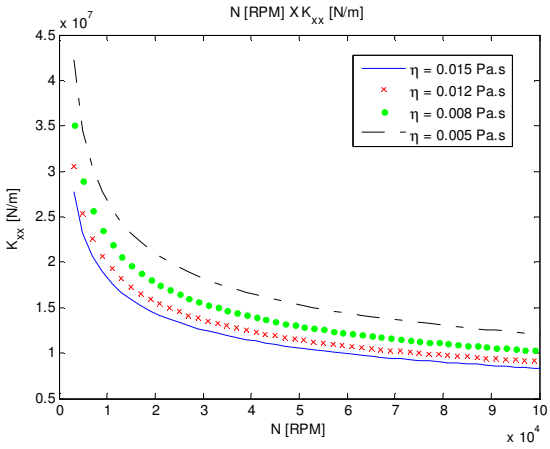

Figure 14. Stiffness coefficients for different values of fluid viscosity

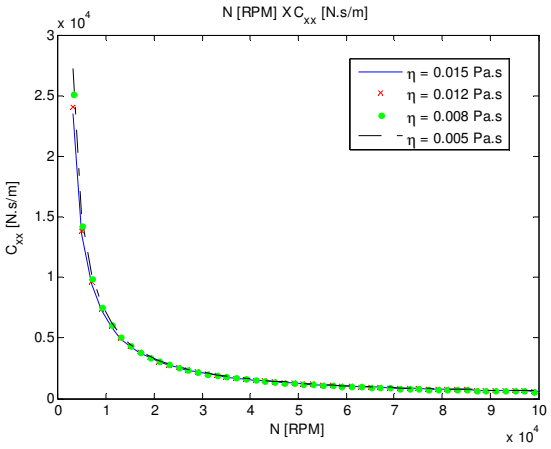

Figure 15. Damping coefficients for different values of fluid viscosity

Figure 14 and Fig. 15 show the behavior of the stiffness and damping coefficients as function of the speed of the shaft for four different values of viscosity of the lubricant. The influence of the viscosity is clear for the stiffness coefficients, showing that for less viscous oils, the stiffness coefficients obtained are higher, since the film thickness required to support the axial load of 100N is thinner, resulting in a stiffer system. With regards to the damping coefficients, the influence of the viscosity, at this specific case, is not expressive and the curves are almost overlapping.

The temperature of the fluid has influence on its viscosity and, as a consequence, on the load capacity of the bearing and the stiffness and damping coefficients. This influence is of great importance at high speeds, in such a way that the temperature of the fluid will increase as the speed increases, causing a reduction of the fluid's viscosity, resulting in the fact that the film thickness necessary to support a defined axial load at a defined speed must be smaller. The influence of the temperature, using a Thermohydrodynamic (THD) model, was analyzed by Daniel et al. (2010) for journal bearings and such analysis is to be performed for thrust bearings in a near future.

2.5.3 Validation and Additional Results

In order to validate the results for stiffness and damping coefficients by the model used in the present paper, some results were obtained for a different geometry of bearing pad and compared to the results from Zhu and Zhang (2003). The bearing pad geometry considered can be seen in Fig. 16. Figure 17 shows the fluid film thickness considered in this case and the angle α, an important variable considered by Zhu and Zhang (2003) in their paper. Three different values of α were used in the analysis, resulting in three different values of $\tan(\alpha)$. A constant speed of 36000RPM and twelve bearing pads with $\theta_o = 25°$ were considered. Other information of the bearing pads can be seen in Zhu and Zhang (2003).

The stiffness and damping coefficients obtained are shown, respectively, in Fig. 18 and Fig 19 (in logarithmic scale, as done by Zhu and Zhang, 2003). The results from Fig. 18, demonstrate that for cases with less inclined ramps (smaller values of $\tan(\alpha)$) the stiffness coefficient is greater then the coefficients obtained for bearing pads with more inclined ramps for a certain range of film thicknesses; at certain point, the curves cross each other (at this particular case, this phenomenon occurs for $h_o \approx 35x10^{-6}$ m) and the bearing with more inclined ramps becomes stiffer than the others.

With regard to the damping coefficients, bearings with less inclined ramps result in higher damping coefficients for the entire range of h_o analyzed.

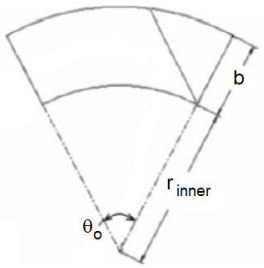

Figure 16. Bearing pad geometry

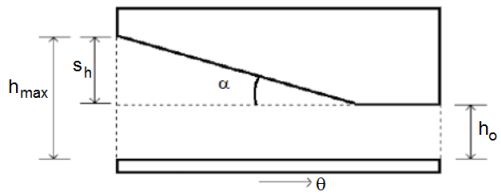

Figure 17. Fluid film thickness and angle α

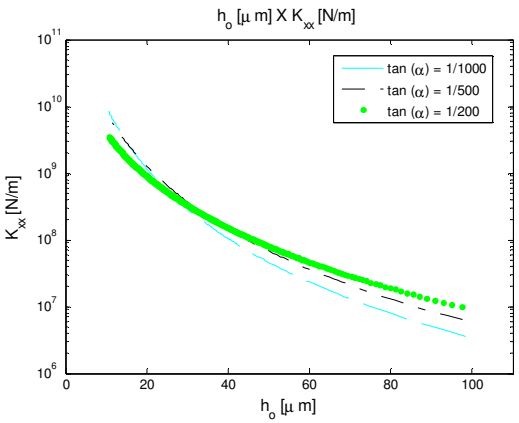

Figure 18. Stiffness coefficients as function of the minimum film thickness for different values of $\tan(\alpha)$

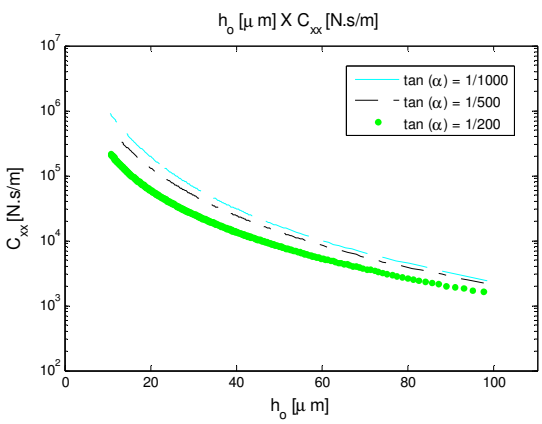

Figure 19. Damping coefficients as function of the minimum film thickness for different values of $\tan(\alpha)$

2.6 CONCLUSIONS

The FVM is proposed to solve the lubrication dynamic model for thrust bearings with grooves, in polar coordinates. The model seems reasonable when comparing its results to those obtained from different models (FDM and Zhu and

Zhang, 2003).

The influence of temperature of the lubricant fluid is not analyzed in the present paper. However, it is know that at higher speeds, the temperature of the fluid increases and its viscosity decreases, causing a reduction at its load capacity. Further analyses of this influence are suggested to be performed in the future.

Impact of important design parameters such as angular extension, inclination of the bearing pad ramp and fluid viscosity of the bearing pad were also discussed and analyzed.

This work showed results that were performed without the consideration of a concentrated inertia term, as done by Arghir et al. (2002) in part of his analyses. The influence of such term at high speeds, however, is recognized to be important and will be analyzed in future works.

3. ACKNOWLEDGEMENTS

The authors thank BorgWarner Brasil Ltda. for the financial and technical support for this research, as well as CNPq, CAPES and FAPESP for research funds.

4. REFERENCES

Arghir, M.; Alsayed, A.; Nicolas, D.; *The Finite Volume Solution of the Reynolds Equation of Lubrication with Film Discontinuities*; International Journal of Mechanical Sciences, Vol. 44, pp. 2119-2132, 2002.

Daniel, G. B.; Alves, D. S.; Cavalca, K. L.; Cruz, R. F.; *Temperature Influence on the Equivalent Coefficients Estimation for Journal Bearings*, In: 2010 STLE Annual Meeting & Exhibition, Las Vegas, Nevada, USA, 2010.

Hamrock, B. J.; Schmid, S. R.; Jacobson, B. O., "Fundamentals of Machine Elements", McGraw Hill, 2nd ed., New York, USA, pp. 325-539, 2005.

Jang, G.; Lee, S.; *Determination of the dynamic coefficients of the coupled journal and thrust bearings by the perturbation method;* Tribology Letters, Vol. 22, Jun 2006.

Kogure, K.; Fukui, S.; Mitsuya, Y.; Kaneko, R.; *Design of Negative Pressure Slider for Magnetic Recording Discs*, ASME Journal of Lubrication Technology, Vol. 105, pp. 496-502, 1983.

Koç, E.; *An Investigation into the Numerical Solution of Reynolds´ Lubrication Equation with Special Reference to Thrust Bearings*, Tribology International, Vol. 230, pp. 429-437, 1990.

Lund, J.; *Review of the Concept of Dynamic Coefficients for Fluid Film Journal Bearings*, ASME Journal of Tribology, Vol. 109, pp. 37- 41, 1987.

Machado, T. H.; Cavalca, K. L.; *Evaluation of Dynamic Coefficients for Fluid Film Journal Bearings with Different Geometries*, In: 20th International Congress of Mechanical Engineering - COBEM 2009, Proceedings of the 20th International Congress of Mechanical Engineering, Gramado, Brazil, 2009.

Petrov, N. P.; *Friction in Machines and the Effect of Lubricant*, Inzenernii Zhurnal, St. Petersburg, Vol. 1, pp. 71-140, Vol. 2, pp. 228-279, Vol. 3, pp. 377-436, Vol. 4, pp. 535-564, 1883.

Pinkus, O.; *Analysis of Elliptical Bearings*, Transactions of the ASME, Vol. 78, pp. 965-973, Jul. 1956.

Pinkus, O.; Lynn, W.; *Solution of the Tapered-Land Sector Thrust Bearing*, Transactions of the ASME, 80, pp. 1510-1516, Oct. 1958.

Reynolds, O.; *On the Theory of Lubrication and its Application to Mr. Beauchamp Tower's Experiments, including an Experimental Determination of the Viscosity of Olive Oil*. Philosophical Transactions of Royal Society of London, Series A, Vol. 177, Part 1, pp. 157-234, 1886.

Singhal, G. C.; *Computational Method for Hydrodinamic Problems (Reynolds' Equation)*, Computer Aided Design, pp. 151-154, 1981.

Storteig, E.; White, M. F.; *Dynamic Characteristics of Hydrodynamically Lubricated Fixed-Pad Thrust Bearings*, WEAR, Vol. 232, pp. 250-255, 1999.

Tower, B.; *Second report on friction experiments*, Proceedings of the Institution of Mechanical Engineers, pp. 58-70, 1885.

Vieira, L. C., Cavalca, K.L.; *Hydrodynamic Lubrication Evaluation of Sector Thrust Bearings*, In: 20th International Congress of Mechanical Engineering - COBEM 2009, Proceedings of the 20th International Congress of Mechanical Engineering, Gramado, Brazil, 2009.

Vieira, L. C., Cavalca, K.L., Nomura, P. O.; *Hydrodynamic Lubrication Evaluation Thrust Bearings*, In: 2010 STLE Annual Meeting & Exhibition, Las Vegas, Nevada, USA, 2010.

Zhu, Q.; Zhang, W. J.; *A Preliminary Nonlinear Analysis of The Axial Transient Response of the Sector-Shaped Hydrodynamic Thrust Bearing-Rotor System*; Transactions of ASME – Journal of Tribology, Vol. 125, pp. 854-858, Oct. 2003.

5. RESPONSIBILITY NOTICE

The authors are the only responsible for the printed material included in this paper.